



### **OPEN ACCESS**

EDITED BY

Gloria María Castellano-Estornell, Catholic University of Valencia San Vicente Mártir. Spain

REVIEWED BY

Feng Tang.

Chinese Academy of Sciences (CAS), China Murali Ragothaman,

University of Oklahoma Health Sciences Center, United States

\*CORRESPONDENCE

Tianjun Liu

☑ liutj@bme.cams.cn

RECEIVED 06 August 2025 REVISED 30 October 2025 ACCEPTED 10 November 2025 PUBLISHED 26 November 2025

### CITATION

Mao L, Zhang Y, Zhu N, Wang X and Liu T (2025) Enhanced therapeutics of cabazitaxel via polycarboxylate conjugation: improved solubility, safety, and antitumor efficacy. *Front. Immunol.* 16:1680710. doi: 10.3389/fimmu.2025.1680710

### COPYRIGHT

© 2025 Mao, Zhang, Zhu, Wang and Liu. This is an open-access article distributed under the terms of the Creative Commons Attribution License (CC BY). The use, distribution or reproduction in other forums is permitted, provided the original author(s) and the copyright owner(s) are credited and that the original publication in this journal is cited, in accordance with accepted academic practice. No use, distribution or reproduction is permitted which does not comply with these terms.

# Enhanced therapeutics of cabazitaxel via polycarboxylate conjugation: improved solubility, safety, and antitumor efficacy

Lina Mao, Yan Zhang, Na Zhu, Xueming Wang and Tianjun Liu\*

Tianjin Key Laboratory of Biomedical Materials, Institute of Biomedical Engineering, Chinese Academy of Medical Sciences and Peking Union Medical College, Tianjin, China

**Introduction:** Cabazitaxel (CTX) is a potent anticancer agent whose clinical utility is severely limited by poor aqueous solubility and severe systemic toxicity. To overcome these challenges, we designed and synthesized two water-soluble polycarboxylate conjugates, CTX-DTPA and CTX-TTHA.

**Methods:** The conjugates were characterized via NMR and mass spectrometry. Their hydrophilicity was assessed by lipid-water partition coefficient. Antitumor activity was evaluated in vitro across multiple cancer cell lines and in vivo using xenograft and immunocompetent models. Mechanisms were investigated via molecular docking, immunofluorescence, and tubulin polymerization assays. Safety profiles were assessed through hemocompatibility, myelosuppression, and thymic toxicity evaluations. Pharmacokinetics and biodistribution were analyzed in SD rats.

**Results:** The derivatives exhibited potent antitumor activity comparable to unmodified CTX, effectively inducing apoptosis and G2/M cell cycle arrest. Mechanistic studies revealed moderately reduced binding affinity to  $\beta$ -tubulin but more sustained microtubule stabilization. Remarkably, the conjugates demonstrated a 64-fold improvement in hemocompatibility, significantly minimized myelosuppression, and preserved thymic architecture and immune function. Pharmacokinetic analysis showed prolonged circulation, efficient clearance, and drastically diminished off-target tissue accumulation for CTX-DTPA.

**Discussion:** This study establishes polycarboxylate conjugation as a promising strategy for developing safer and more effective chemotherapeutic agents through rational molecular design, successfully decoupling antitumor efficacy from systemic toxicity.

### KEYWORDS

cabazitaxel, polycarboxylic acid modification, microtubule stabilization, thymic toxicity, tumor targeting

# 1 Introduction

Cabazitaxel (CTX), a potent semi-synthetic microtubule inhibitor, is a key therapeutic option for treating advanced, taxane-resistant cancers (1–4). However, its formidable clinical utility is severely hampered by formulation challenges stemming from an inherent lack of aqueous solubility (5). The requisite solubilizing agents, polysorbate 80 and ethanol, are not pharmacologically inert; they are directly implicated in a spectrum of serious adverse effects, including acute hemolysis, hypersensitivity reactions, and cumulative organ toxicity, which collectively contribute to narrow therapeutic index of CTX (6).

In response, the scientific community has largely pursued a drug delivery system (DDS) paradigm (7–10). Strategies such as lipid emulsions (11, 12), polymeric nanoparticles (13, 14), albumin-bound complexes (15), and various other nanocarriers have been explored to physically encapsulate CTX (16). While preclinical successes have been reported, these carrier-based approaches often have intrinsic limitations: complex and poorly reproducible manufacturing, low drug-loading capacity, instability during storage leading to premature drug release, and potential immunogenicity of the carrier materials themselves (17–20). These challenges underscore that physical encapsulation may not be the most robust or clinically translatable path forward.

Herein, we propose a paradigm shift from physical encapsulation to rational chemical redesign. Instead of constructing a vehicle for the drug, we directly engineered the drug molecule itself. We report a novel strategy of polycarboxylic acid conjugation to create two inherently water-soluble CTX derivatives: CTX-DTPA and CTX-TTHA. This chemical modification fundamentally alters the hydrophilicity of CTX, transforming it into a new molecular entity that eliminates the need for toxic solvents or complex nanocarriers.

In addition to addressing the paramount issue of solubility, this study rigorously investigated whether this structural redesign can dissociate the antitumor efficacy of CTX from its systemic toxicity. We place particular emphasis on thymic toxicity—a critical yet underappreciated side effect of taxane therapy that can compromise long-term immune competence. Through comprehensive *in vitro* and *in vivo* evaluations, we demonstrate that this conjugation strategy not only preserves potent anticancer activity but also confers a dramatically enhanced safety profile, offering a promising blueprint for next-generation, immunocompatible chemotherapeutics.

Methods

# 1.1 Synthesis of CTX-TTHA or CTX-DTPA

The CTX-TTHA and CTX-DTPA conjugates were synthesized through polycarboxylic acid conjugation. First, triethylenetetraminehexaacetic acid (TTHA, 1.48 g) was activated with acetic anhydride (2 mL) and pyridine (1.89 g) at 45°C for 4 h. The intermediate was washed with acetic anhydride and ether, then dried under vacuum. For conjugation, the activated intermediate (0.45 g) was dissolved in DMF with Na<sub>2</sub>SO<sub>4</sub>•10H<sub>2</sub>O (0.035 g) at 70°C for 4 h, followed by addition of cabazitaxel (0.75 g), DMAP

(0.012 g), and TEA (140  $\mu$ L) with 24 h stirring. The products were precipitated with cold ether and purified by semi-preparative HPLC, yielding >97% pure conjugates as confirmed by  $^1H$  NMR and mass spectrometry. Diethylenetriaminepentaacetic acid (DTPA) was treated following the identical procedure.

# 1.2 Lipid-aqueous partition coefficient

CTXs were dissolved in octanol, and an equal volume of water was added, followed by shaken at 100 rpm for 24 h at room temperature. The upper octanol phase and lower water phase were separated by centrifugation. The supernatant was analyzed by HPLC (Bruker SolanX 70 FT-MS; Agilent 6540TOF) (21).

# 1.3 Cytotoxicity

Human cancer cell lines were cultured in basic medium (10% fetal bovine serum (FBS)+1% double antibody solution) (Biological Industries) at  $37^{\circ}$ C in a 5% CO<sub>2</sub> incubator. Effects of CTXs on cell proliferation and viability were measured by an MTS (Promega Corporation) assay. Absorbance values at 490 nm were measured using a microplate reader (Thermo Scientific, Varioskan Flash) (22).

# 1.4 Cell cycle arrest

Cells were incubated with drugs for 24 h. Fixed cells were incubated with RNase A and stained with propidium iodide (PI). DNA content was determined in a flow cytometer (BD FACS CaliburTM Flow Cytometer, USA) (23).

# 1.5 Molecular docking simulations

The molecular interactions between cabazitaxel (CTX) derivatives and human  $\beta$ -tubulin isotypes were investigated through molecular docking simulations using AutoDock 4.2 software (24). The crystal structure of human  $\beta$ -tubulin (PDB ID: 5SYF; resolution: 3.5 Å) was obtained from the RCSB Protein Data Bank. Structural preparation involved: (1) removal of water molecules and heteroatoms using PyMOL 2.5.2, and (2) addition of polar hydrogen atoms and assignment of Gasteiger charges using AutoDock Tools 1.5.7.

Prior to docking, all CTX derivatives were energy-minimized and converted to PDBQT format using Chem3D and AutoDock Tools, with rotatable bonds properly defined. Docking simulations were performed with AutoDock Vina 1.2.0 employing a semiflexible approach (rigid protein, flexible ligands). A grid box of dimensions  $39.8 \times 40.5 \times 42.0 \text{ Å}^3$  was centered on the binding pocket coordinates (x = 327.007, y = 461.105, z = 364.004). Key docking parameters included: exhaustiveness = 32, number of modes = 10, and energy range = 3.0 kcal/mol.

The docking protocol was validated through redocking of the native ligand, yielding an acceptable root-mean-square deviation (RMSD) of 1.5 Å. The lowest-energy conformation from each docking simulation was selected for detailed interaction analysis, with molecular visualization and analysis performed using PyMOL.

## 1.6 Immunofluorescence

DU145 and PC-3 cells were fixed, and incubated with the rabbit monoclonal anti- $\alpha$  tubulin antibody (1:400, ab52866; Abcam) for 1 h, and thereafter with Alexa Fluor 488 conjugated goat anti-rabbit secondary antibody (1:500, ZF-0511; ZSGB-BIO) for 1 h. After DAPI staining, the fluorescently stained cells were visualized by confocal microscopy (Zeiss LSM710, Germany).

# 1.7 Purified tubulin polymerization

A tubulin polymerization assay kit (Cytoskeleton, BK006P) was used. Briefly, 10  $\mu$ l of CTXs with a concentration of 100  $\mu$ M in the general tubulin buffer and 100  $\mu$ l of tubulin (3 mg/ml) in TP buffer were added on ice. The 96-well plate was immediately placed in a microplate reader at 37°C.

# 1.8 Hemolysis test

The hemolytic potential of CTX formulations was evaluated using rat red blood cells (RBCs). Briefly, whole blood was collected from the abdominal aorta of anesthetized SD rats into ACD anticoagulant (blood:ACD = 1:4, v/v). The blood was diluted with normal saline (4:5, v/v) and centrifuged at 450 g for 10 min. The RBC pellet was washed three times with normal saline until the supernatant was clear. The washed RBCs were then resuspended in normal saline to prepare a 2% (v/v) suspension.

For the assay, 500  $\mu L$  of the 2% RBC suspension was mixed with an equal volume of serially diluted drugs or controls in 1.5 mL tubes. The controls included: Negative control (0% hemolysis): normal saline. Positive control (100% hemolysis): distilled water. Solvent control: the vehicle for unmodified CTX (2.5% Tween 80 + 2.5% anhydrous ethanol + 95% normal saline). The mixtures were incubated at 37 °C for 1.5 h and then centrifuged at 450 g for 5 min. Subsequently, 150  $\mu L$  of the supernatant from each tube was transferred to a 96-well plate, and the absorbance at 545 nm (OD545) was measured using a microplate reader. The percentage of hemolysis was calculated using the following formula: Hemolysis (%) = [(OD545) was measured using the following formula: Hemolysis (%) = [(OD545) was measured using the following formula: Hemolysis (%) = [(OD545) was measured using the following formula: Hemolysis (%) = [(OD545) was measured using the following formula: Hemolysis (%) = [(OD545) was measured using the following formula: Hemolysis (%) = [(OD545) was measured using the following formula: Hemolysis (%) = [(OD545) was measured using the following formula: Hemolysis (%) = [(OD545) was measured using the following formula: Hemolysis (%) = [(OD545) was measured using the following formula: Hemolysis (%) = [(OD545) was measured using the following formula: Hemolysis (%) = [(OD545) was measured using the following formula: Hemolysis (%) = [(OD545) was measured using the following formula: Hemolysis (%) = [(OD545) was measured using the following formula: Hemolysis (%) = [(OD545) was measured using the following formula: Hemolysis (%) = [(OD545) was measured using the following formula: Hemolysis (%) = [(OD545) was measured using the following formula: Hemolysis (%) = [(OD545) was measured using the following formula: Hemolysis (%) = [(OD545) was measured using the following formula: Hemolysis (%) = [(OD545) was measured using the following formula: Hemolysis (%) = [(OD545) was measured using the following formula: Hemol

# 1.9 Tumor models and drug administration

All animal experiments were conducted in accordance with protocols approved by the Institutional Animal Care and Use Committee of Peking Union Medical College. Male BALB/c nude

mice (6–8 weeks old) and female KM mice (6–8 weeks old) were purchased from Charles River Laboratories (Beijing, China) and maintained under specific pathogen-free conditions. Drug doses were optimized based on preliminary toxicity studies to achieve comparable therapeutic effects across different tumor models.

DU145 Prostate cancer model: DU145 cells (3×106 cells/mouse) were subcutaneously inoculated into the right flank of BALB/c nude mic. When tumors reached approximately 100 mm³, mice were randomly divided into four treatment groups (n=6/group): (a) Vehicle control; (b) CTX (3  $\mu$ mol/kg); (c) CTX-TTHA (3  $\mu$ mol/kg); (d) CTX-DTPA (3  $\mu$ mol/kg). Treatments were administered via tail vein injection three times at 3-day intervals. Major organs were collected for histopathological examination after the final administration.

MCF-7 Breast Cancer Model: Female BALB/c nude mice bearing MCF-7 xenografts ( $2\times10^6$  cells/mouse) were randomized into treatment groups as described above, with an adjusted dose of 9.6  $\mu$ mol/kg for all CTX formulations.

H22 hepatoma model: Female KM mice were subcutaneously implanted with H22 cells ( $2\times10^6$  cells/mouse) and assigned to six groups: (a) Vehicle control; (b) CTX (9.6  $\mu$ mol/kg in 5% glucose with 2.5% ethanol/2.5% Tween 80); (c) CTX-TTHA (9.6  $\mu$ mol/kg in saline); (d) CTX-DTPA (9.6  $\mu$ mol/kg in saline); (e) CTX-TTHA (19.1  $\mu$ mol/kg in saline); (f) CTX-DTPA (19.1  $\mu$ mol/kg in saline).

Treatments were administered every other day for four doses (three doses for CTX group due to weight loss >15%). Peripheral blood samples were collected for complete blood count analysis using an automated hematology analyzer.

Drug doses were optimized based on preliminary toxicity studies and the principle of molar equivalence to achieve comparable therapeutic effects across different tumor models. The doses for CTX-DTPA and CTX-TTHA were calculated to deliver an equimolar amount of the cabazitaxel moiety relative to the unmodified CTX.

## 1.10 Thymic cell apoptosis analysis

Gently mix  $1\times10^6$  thymocytes with FITC Anexin V (5  $\mu$ l) and PI (10  $\mu$ l), and incubate in the dark for 15 minutes, RT. Analyze by flow cytometry. Thymocytes were stained with anti-mouse CD3e cyanine 5.5 (eBioscience, 85-45-0031-82), anti-CD4 PE (eBioscience, 85-12-0042-82), anti-CD8a FITC (4°C 30 min) and detected by flow cytometry.

### 1.11 Pharmacokinetic methods

Male and female SD rats (200–220 g) received intravenous injections of CTX or CTX-DTPA (6  $\mu$ mol/kg). CTX was dissolved in 2.5% Tween 80/2.5% EtOH/saline, while CTX-DTPA used saline alone. Blood samples were collected at 5 min to 24 h post-dose. Tissues (heart, liver, spleen, lung, kidney, thymus) and excreta were collected at 15 min, 2 h, 4 h, and 12 h. Plasma and tissue samples were processed by liquid-liquid extraction with n-butanol and analyzed via

LC-MS/MS (Agilent Poroshell 120 EC-C18 column; 0.05% formic acid/acetonitrile gradient). Pharmacokinetic parameters were calculated using DAS 2.0 via non-compartmental analysis.

# 1.12 Statistical analysis

All the data were expressed as mean  $\pm$  SD, and a one-way analysis of variance (ANOVA) was performed. P<0.05 was considered to be statistically significant.

# 2 Results

# 2.1 Synthesis of the CTX-TTHA and CTX-DTPA conjugates

The water-soluble CTX derivatives, CTX-DTPA and CTX-TTHA, were successfully synthesized through polycarboxylic acid conjugation (Figure 1a). Structural confirmation of the synthesized compounds was achieved using <sup>1</sup>H NMR spectroscopy (Figure 1c) and mass spectrometry (Supplementary Figures S1, S2). The <sup>1</sup>H

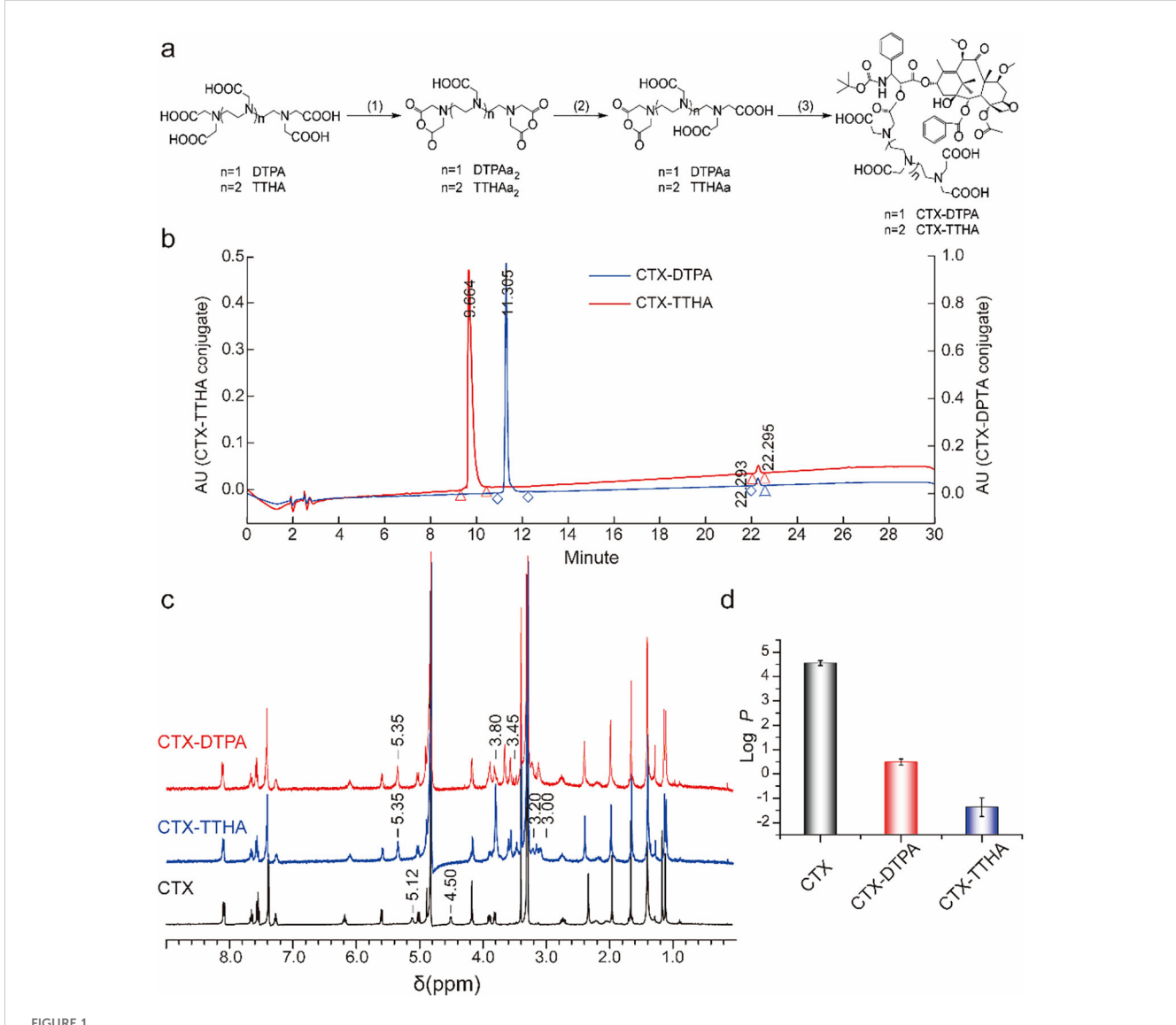


FIGURE 1
Compounds CTX-TTHA and CTX-DTPA. (a) Synthesis of water-soluble cabazitaxel compounds. Note for reagents and conditions. (1) Acetic anhydride, pyridine, 45°C, 4 h. (2) Dimethylformamide, 70°C, 4 h. (3) Cabazitaxel, 4-dimethylaminopyridine, triethyl amine, RT, 24 h. (b) HPLC trace of CTX-DTPA and CTX-TTHA conjugate. Running in a Waters C18 column (Kromasil, 5μm, 4.6 × 250 mm) with a flow of 1 mL/min of 0.05% methanoic acid in acetonitrile. The HPLC data was quantified by the integrated area under the peak at an absorbance of 227 nm. 1H NMR (400 MHz, Methanol-D4) (c) and lipid water distribution coefficients (d) of CTXs.

NMR spectra revealed a notable downfield shift of the -CH proton signal at the 2'-position of cabazitaxel, from 5.12 ppm (CTX) to 5.35 ppm (CTX-DTPA) or 5.35 ppm (CTX-TTHA). Concurrently, the characteristic hydroxyl proton peak at 4.50 ppm (2'-OH) in CTX disappeared in the derivatives, while new peaks emerged at 3.45–3.80 ppm and 3.00–3.20 ppm, corresponding to the -N-CH<sub>2</sub>-COOH- and -N-CH<sub>2</sub>-CH<sub>2</sub>-N- moieties of the DTPA and TTHA frameworks, respectively.

HPLC analysis confirmed the high purity of the conjugates (~97%, Figure 1b), with MALDI-TOF mass spectrometry yielding the following molecular ions: [CTX-DTPA-Na]<sup>+</sup> at m/z 1233.4953, [CTX-DTPA-2Na]<sup>+</sup> at m/z 1255.4793 (Supplementary Figure S1), [CTX-TTHA-Na]<sup>+</sup> at m/z 1334.5429, and [CTX-TTHA-2Na]<sup>+</sup> at m/z 1356.5824 (Supplementary Figure S2).

The lipid-water partition coefficient assay demonstrated a significant enhancement in hydrophilicity for the derivatives. The logP values decreased from 4.55  $\pm$  0.10 (CTX) to 0.49  $\pm$  0.12 (CTX-DTPA) and -1.37  $\pm$  0.38 (CTX-TTHA) (Figure 1d), confirming the order of water solubility as CTX < CTX-DTPA < CTX-TTHA. These results demonstrate that polycarboxylic acid modification significantly improves the aqueous solubility of cabazitaxel while preserving its structural integrity.

# 2.2 *In vitro* anticancer efficacy of CTX derivatives

The cytotoxic effects of CTX-DTPA and CTX-TTHA were evaluated across a panel of human cancer cell lines (A549, Bel-7402, DU145, Fadu, H358, H460, H520, HCT116, HT-29, LN229, MCF-7, PC-3, SK-OV-3) and two normal cell lines (L-02, 3T3). Both derivatives exhibited dose-dependent cytotoxicity comparable to unmodified CTX, with no statistically significant differences in IC50 values (p > 0.05) (Table 1). These results confirm that polycarboxylate conjugation preserves the antitumor potency of cabazitaxel *in vitro*.

# 2.3 Cell cycle arrest induced by CTX derivatives

To investigate the impact of CTX-DTPA and CTX-TTHA on cell cycle progression, DU145 and MCF-7 cells were treated with varying concentrations (1–25 nM) of the derivatives and analyzed via flow cytometry. Both compounds induced dose-dependent G2/M phase arrest, mirroring the effects of unmodified CTX (Figure 2).

In DU145 cells, treatment with 1 nM CTX-DTPA or CTX-TTHA resulted in the arrest of 16.4  $\pm$  1.0% and 15.1  $\pm$  0.1% of the cells in G2/M, respectively, which was comparable to that observed with CTX (16.5  $\pm$  0.7%). At the higher concentration of 25 nM, G2/M arrest increased significantly to 58.9  $\pm$  16.1% (CTX-DTPA) and 69.9  $\pm$  12.6% (CTX-TTHA), closely matching the effect of CTX (65.5  $\pm$  19.9%) (Figures 2a, c).

TABLE 1 IC<sub>50</sub> of CTXs on cells (nM).

Cells		СТХ	CTX- DTPA	CTX- TTHA
Tumor cell lines	A549	2.5 ± 1.2	3.0 ± 1.1	3.3 ± 1.6
	Bel-7402	2.8 ± 0.5	2.9 ± 0.9	2.4 ± 0.4
	DU145	6.1 ± 2.4	5.1 ± 1.4	4.1 ± 2.2
	Fadu	1.6 ± 0.4	1.9 ± 0.6	2.3 ± 0.9
	H358	1.2 ± 0.6	1.6 ± 0.7	1.6 ± 0.4
	H460	2.4 ± 1.3	2.4 ± 1.1	1.9 ± 0.7
	H520	1.5 ± 0.7	2.0 ± 1.3	2.1 ± 0.6
	HCT 116	2.2 ± 1.1	3.7 ± 1.0	2.1 ± 0.9
	HT-29	7.4 ± 3.4	6.7 ± 2.9	8.4 ± 3.8
	LN229	8.5 ± 2.3	5.8 ± 2.2	7.6 ± 3.1
	MCF-7	5.3 ± 1.9	6.8 ± 2.4	5.5 ± 2.3
	PC-3	5.2 ± 1.7	4.1 ± 0.7	7.4 ± 2.8
	SK-OV-3	4.4 ± 0.9	5.4 ± 1.3	3.2 ± 0.8
Non-tumor cell lines	L-02	7.8 ± 1.5	8.8 ± 3.6	6.8 ± 0.4
	3T3	8.7 ± 3.2	8.3 ± 2.7	8.0 ± 3.3

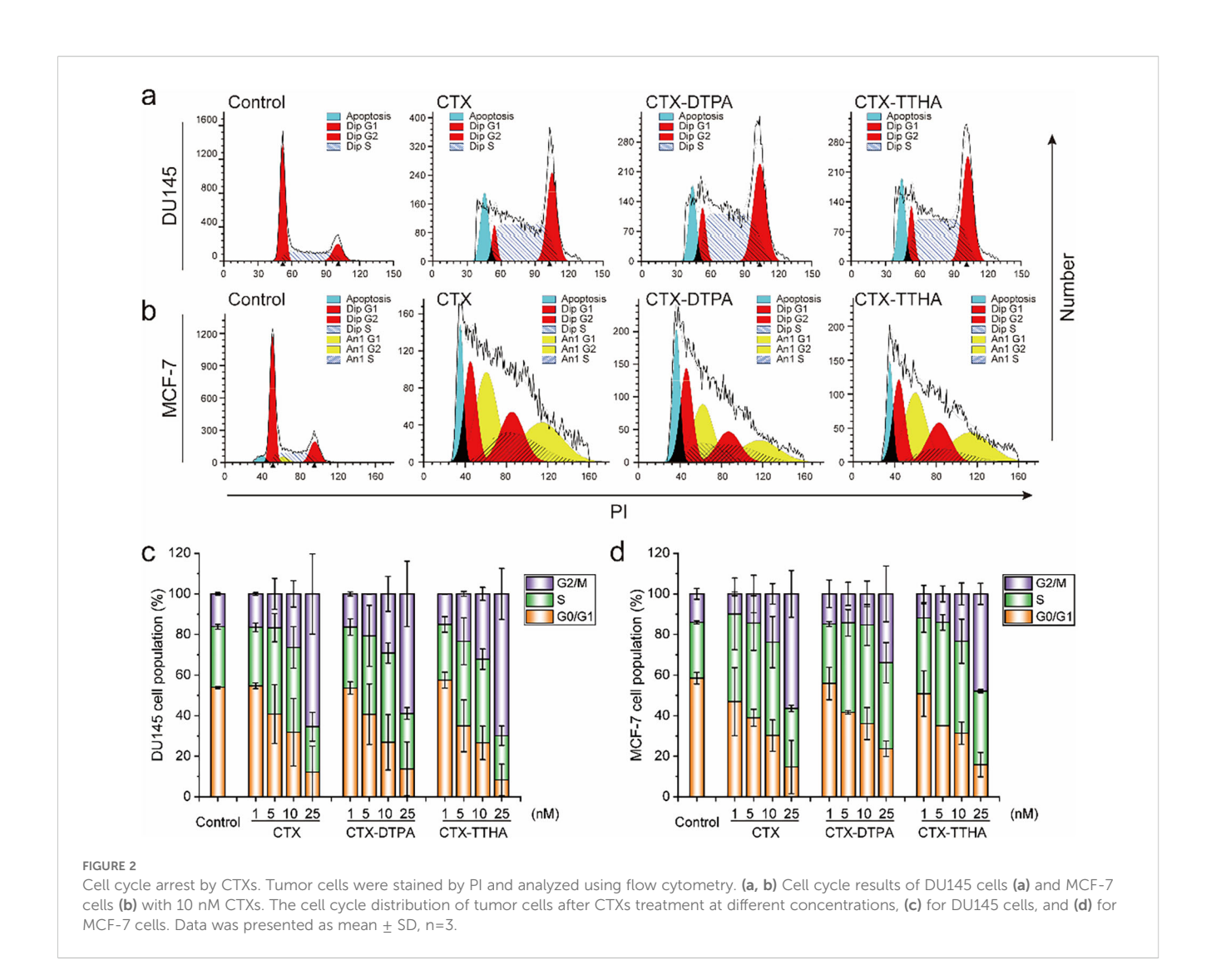
Data was presented as mean  $\pm$  SD, n=3.

Notably, in MCF-7 cells, the derivatives not only induced G2/M arrest but also promoted an euploidy (Figures 2b, d, Supplementary Figure S3), suggesting additional disruption of mitotic fidelity. These results demonstrate that polycarboxylate conjugation preserves the ability of CTX to interfere with microtubule dynamics, leading to cell cycle arrest and aberrant chromosome segregation.

# 2.4 Molecular docking and microtubule interaction studies

Molecular docking analysis revealed distinct binding profiles between native cabazitaxel (CTX) and its polycarboxylate-modified derivatives (CTX-DTPA and CTX-TTHA) with  $\beta$ -tubulin (Figure 3a). The unmodified CTX exhibited the strongest binding affinity (docking score: -8.37 kcal/mol), mediated through three critical interactions: (i) a 2.11 Å hydrogen bond between the C2'-hydroxyl group and Thr274, (ii) extensive hydrophobic contacts with His227, Pro272, and Arg276 residues, and (iii) stabilizing van der Waals interactions with Gly360 and Arg359. These molecular interactions collectively contribute to CTX's potent microtubule-stabilizing activity.

Comparative analysis showed that the water-soluble derivatives maintained binding at the taxane site but with reduced affinities (CTX-DTPA: -5.80 kcal/mol; CTX-TTHA: -5.82 kcal/mol). Structural evaluation revealed that CTX-DTPA's diethylenetriaminepentaacetic acid moiety caused complete loss of the Thr274 hydrogen bond due to steric constraints, while CTX-TTHA retained partial binding through a conserved His227 interaction (2.33 Å), albeit with compromised hydrophobic contacts. This calculated reduction in binding energy



represents an intentional molecular trade-off to achieve superior pharmacokinetic properties.

Immunofluorescence studies revealed that 10 nM concentrations of both derivatives effectively disrupted microtubule networks in DU145 and MCF-7 cells (Figure 3b), inducing characteristic taxane effects including multinuclear formation and aberrant mitotic spindle organization. These cellular observations correlated well with tubulin polymerization assays, which showed that while all compounds enhanced nucleation phase kinetics, the derivatives exhibited more sustained stabilization patterns compared to the transient hyperpolymerization induced by unmodified CTX (Figure 3c). Notably, CTX-DTPA demonstrated polymerization kinetics (43.7  $\pm$  8.0 mOD/min) comparable to paclitaxel, suggesting that polycarboxylate modification transforms CTX's interaction with tubulin to produce more classical microtubule-stabilizing behavior.

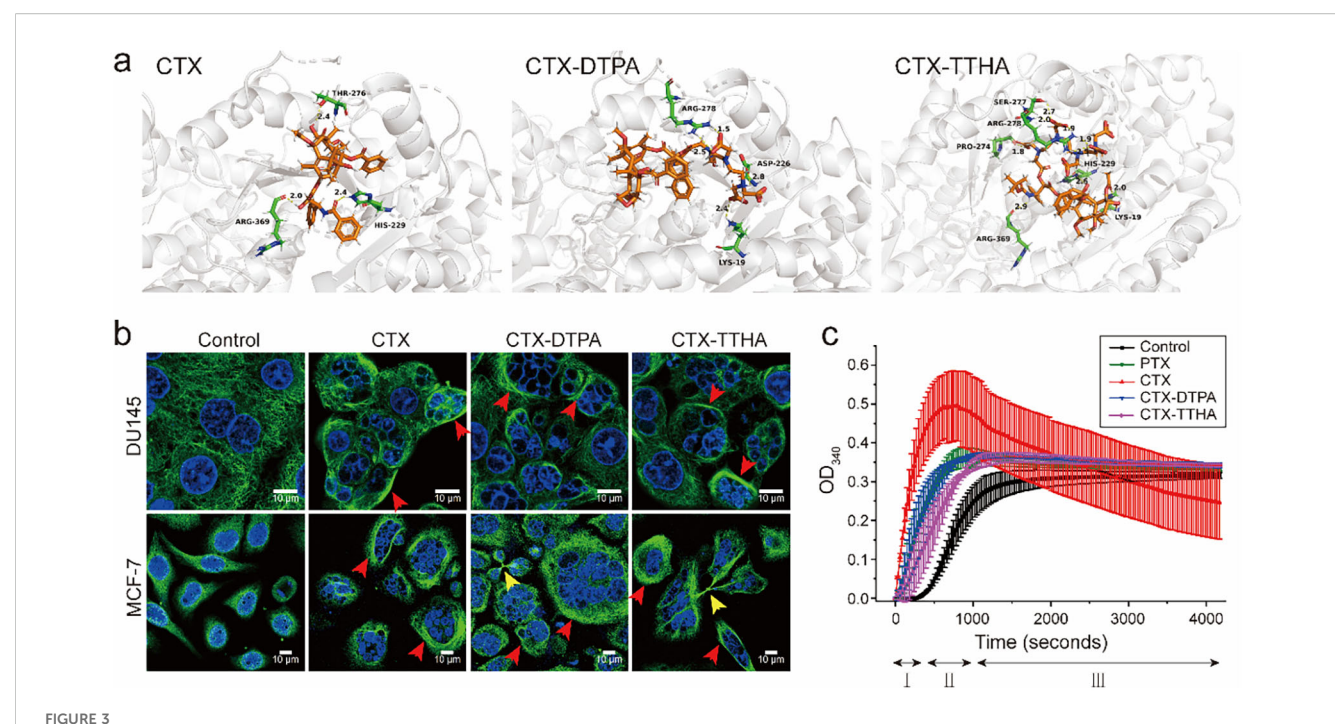
These findings collectively demonstrate that while polycarboxylate conjugation modestly reduces tubulin binding affinity, it preserves the essential microtubule-targeting activity of CTX while conferring improved water solubility and altered polymerization dynamics. The derivatives' ability to maintain antitumor efficacy despite reduced binding energy may be attributed to their enhanced cellular uptake

and sustained drug release properties, as evidenced by the pharmacokinetic studies.

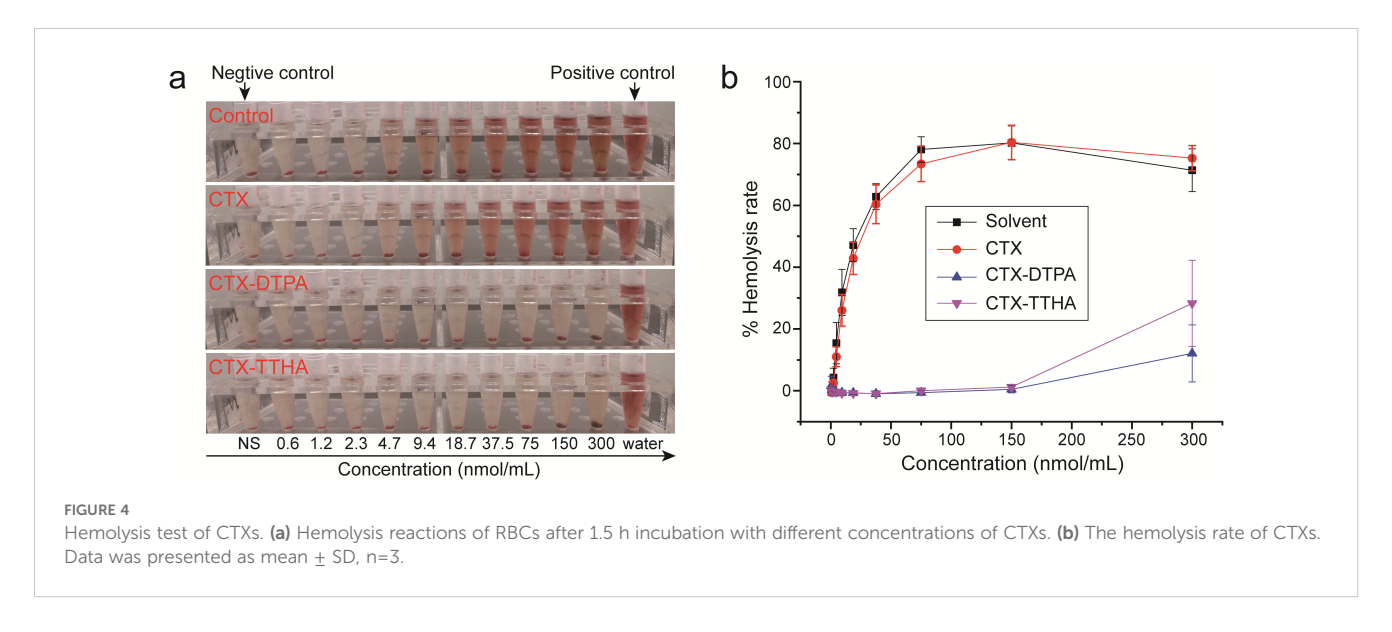
### 2.5 Ex vivo hemocompatibility assessment

The hemolytic potential of CTX derivatives was systematically evaluated using an ex vivo model of rat erythrocytes (Figure 4). Concentration-dependent analysis revealed striking differences in blood compatibility between the parent compound and its modified derivatives. Native CTX exhibited significant hemolytic activity, with hemolysis rates escalating from  $11.0 \pm 3.2\%$  at 4.7 nmol/mL to  $73.4 \pm 5.8\%$  at 75 nmol/mL.

In marked contrast, both CTX-DTPA and CTX-TTHA demonstrated substantially improved hemocompatibility profiles. The derivatives showed negligible hemolysis (<2%) at concentrations up to 150 nmol/mL - a 64-fold improvement over unmodified CTX. Even at the maximum tested concentration of 300 nmol/mL, hemolysis rates remained modest (12.1  $\pm$  9.2% for CTX-DTPA and 28.3  $\pm$  13.9% for CTX-TTHA), representing a dramatic reduction in erythrocyte membrane disruption compared to the parent compound.



Effect on microtubules. (a) Molecular docking models of CTX derivatives with binding pocket of  $\beta$ -tubulin (PDBID: 5syf). Hydrogen bonds are represented by yellow dashed lines, with corresponding bond lengths labeled numerically. (b) Fluorescent micrographs of immunostaining for  $\alpha$ -tubulin of DU145 and MCF-7 cells. Tumor cells treated with CTX, CTX-DTPA, and CTX-TTHA were stained with  $\alpha$ -tubulin antibody (green), and DAPI (blue). The multinuclear structure was visualized, and polymerized microtubule bundles (red arrows) and multipolar splitting (yellow arrows) were indicated. Scale bar, 20  $\mu$ m. (c) Tubulin polymerization reactions of CTXs. The control group illustrated the three phases of polymerization: I (nucleation), II (growth), III (steady-state). Data was presented as mean  $\pm$  SD, n=3.

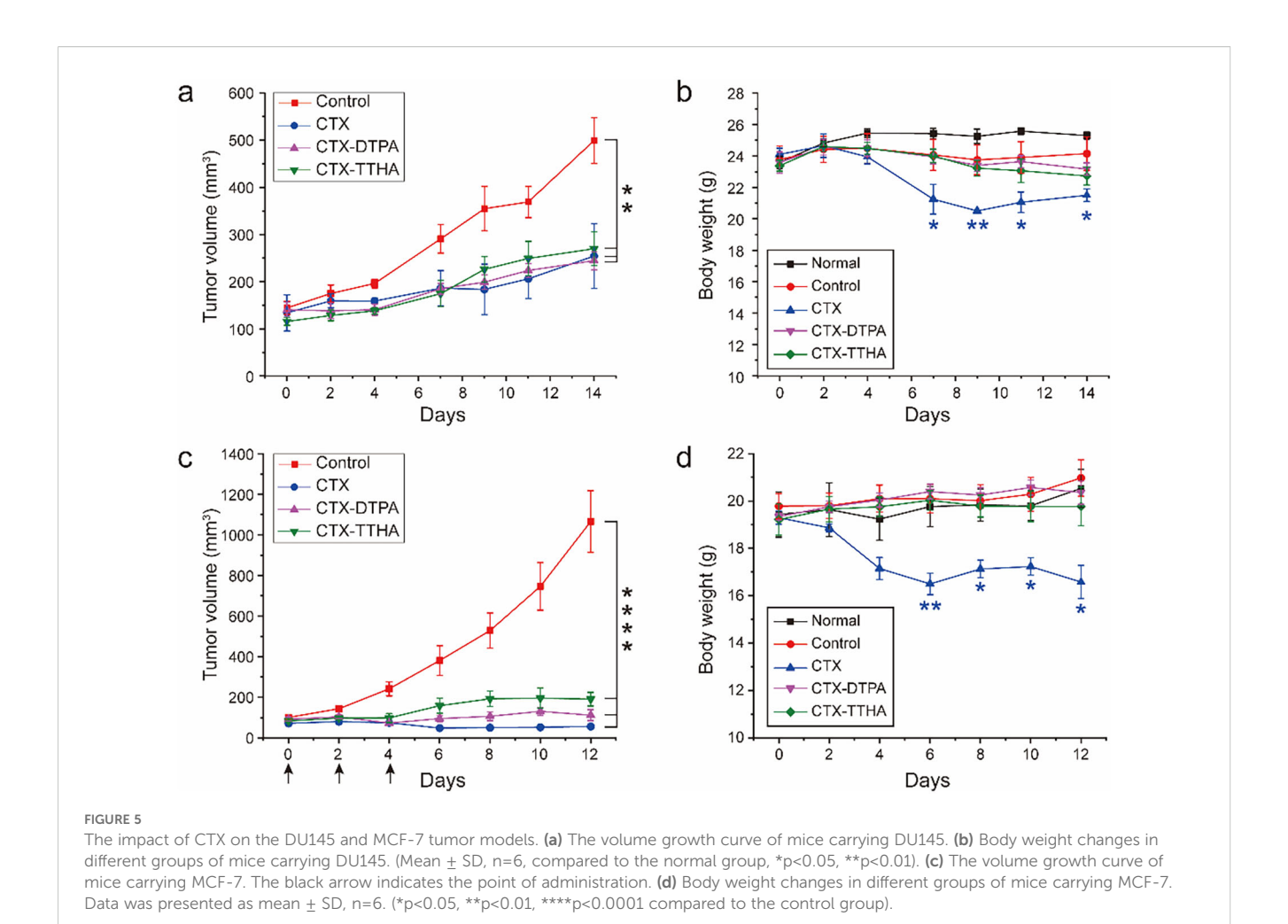


# 2.6 Therapeutic efficacy and safety profile of CTX derivatives in immunodeficient mouse models

We conducted comprehensive evaluations of CTX-DTPA and CTX-TTHA using two well-established xenograft models. In the DU145 prostate cancer model, all treatment groups exhibited significant tumor growth inhibition (p<0.01 versus vehicle

control), with final tumor volumes of 244  $\pm$  32 mm³ (CTX-DTPA), 270  $\pm$  28 mm³ (CTX-TTHA), and 254  $\pm$  35 mm³ (CTX), compared to 500  $\pm$  45 mm³ in controls (Figure 5a). This comparable efficacy profile confirms that structural modification preserves the antitumor activity of the parent compound.

The safety advantages of the derivatives became particularly evident in longitudinal monitoring. While CTX treatment caused >15% body weight loss by day 7, both modified compounds



maintained animal weights within normal physiological ranges (Figure 5b).

In the MCF-7 breast cancer model, we observed tumor volume reductions to  $111 \pm 18$  mm³ (CTX-DTPA) and  $190 \pm 22$  mm³ (CTX-TTHA) versus  $56 \pm 12$  mm³ for CTX at study endpoint (Figure 5c). The complete survival (100%) in derivative-treated groups compared to 83.3% survival with CTX (1/6 mortality) further highlights the enhanced safety profile. Notably, CTX-DTPA showed particularly promising results, achieving near-equivalent efficacy to CTX while completely avoiding the cardiac hypertrophy observed with the parent compound (Supplementary Figure S4). Throughout the treatment period, both CTX-DTPA and CTX-TTHA maintained stable body weights in MCF-7 tumor-bearing mice (Figure 5d), further confirming their improved safety profile over the unmodified CTX.

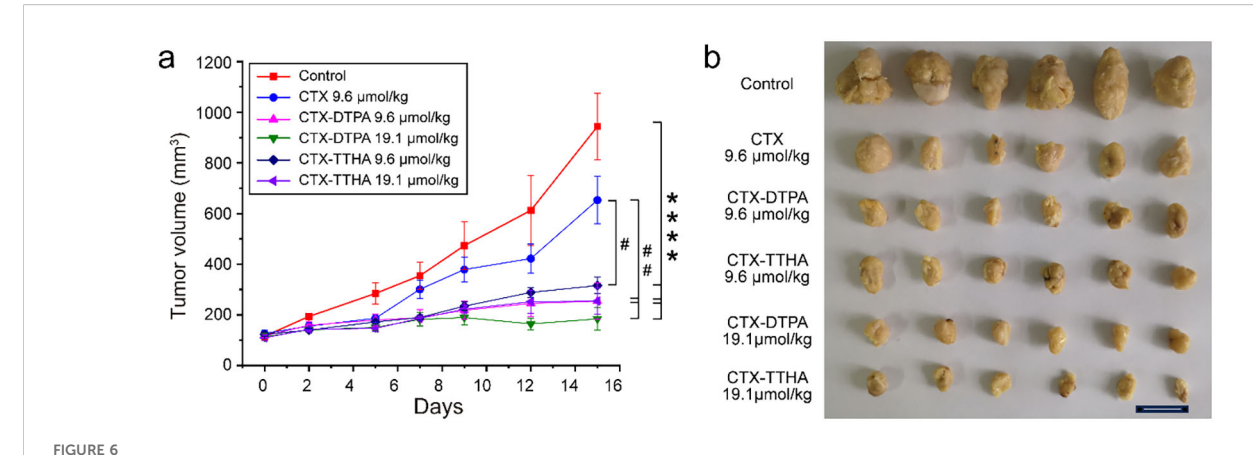
# 2.7 Therapeutic efficacy and safety evaluation in immunocompetent H22 tumor-bearing mice

The antitumor efficacy of CTX derivatives was systematically evaluated in immunocompetent KM mice bearing H22 hepatocellular carcinoma tumors. Treatment with CTX-DTPA

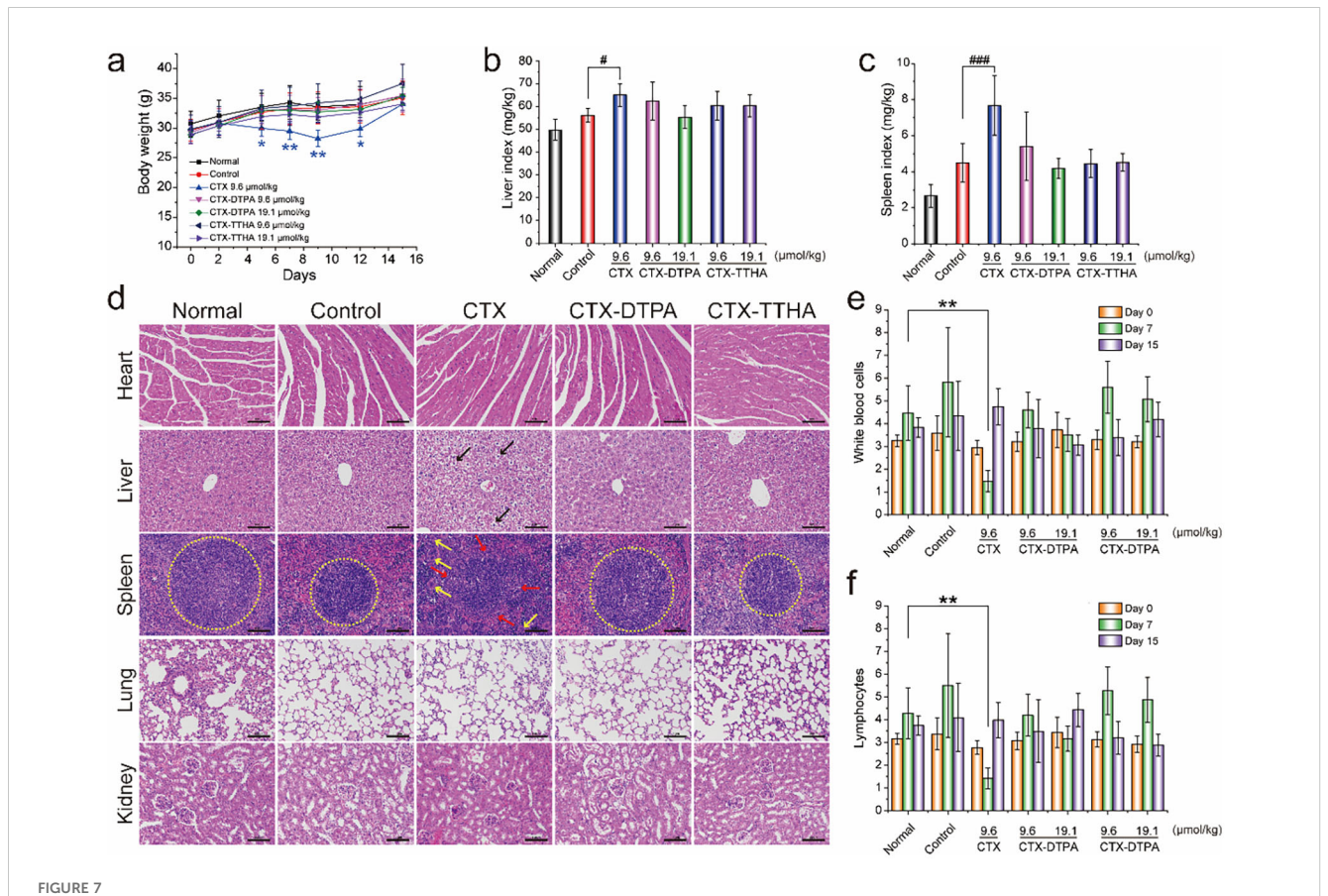
and CTX-TTHA at both standard (9.6  $\mu$ mol/kg) and high (19.1  $\mu$ mol/kg) doses demonstrated significant dose-dependent tumor growth inhibition compared to vehicle controls. Particularly noteworthy was the superior efficacy of high-dose CTX-DTPA, which achieved 80.5% tumor growth inhibition compared to the 30.8% inhibition observed with conventional CTX treatment. Macroscopic examination of excised tumors at study termination confirmed these quantitative findings (Figure 6).

# 2.8 Systemic toxicity evaluation in H22 tumor-bearing mice

The *in vivo* toxicity profiles of CTX-DTPA and CTX-TTHA were comprehensively assessed in immunocompetent H22 tumorbearing mice. Animals treated with unmodified CTX exhibited significant (p<0.05) body weight loss (11-16%) and hepatosplenic toxicity, as evidenced by increased organ indices and histopathological abnormalities including ballooning hepatocyte degeneration and disruption of splenic architecture (Figures 7a-d). In striking contrast, both polycarboxylate-modified derivatives demonstrated markedly improved safety profiles at equivalent therapeutic doses.



The effect of CTXs on H22 tumor model. (a) H22 tumor volume changes. Data was presented as mean  $\pm$  SD, n=6 \*\*\*\*p<0.0001 vs. normal group, #p<0.05 vs. CTX group, ##p<0.01 vs. CTX group. (b) Macroscopic vies of implanted H22 tumors after treatment.

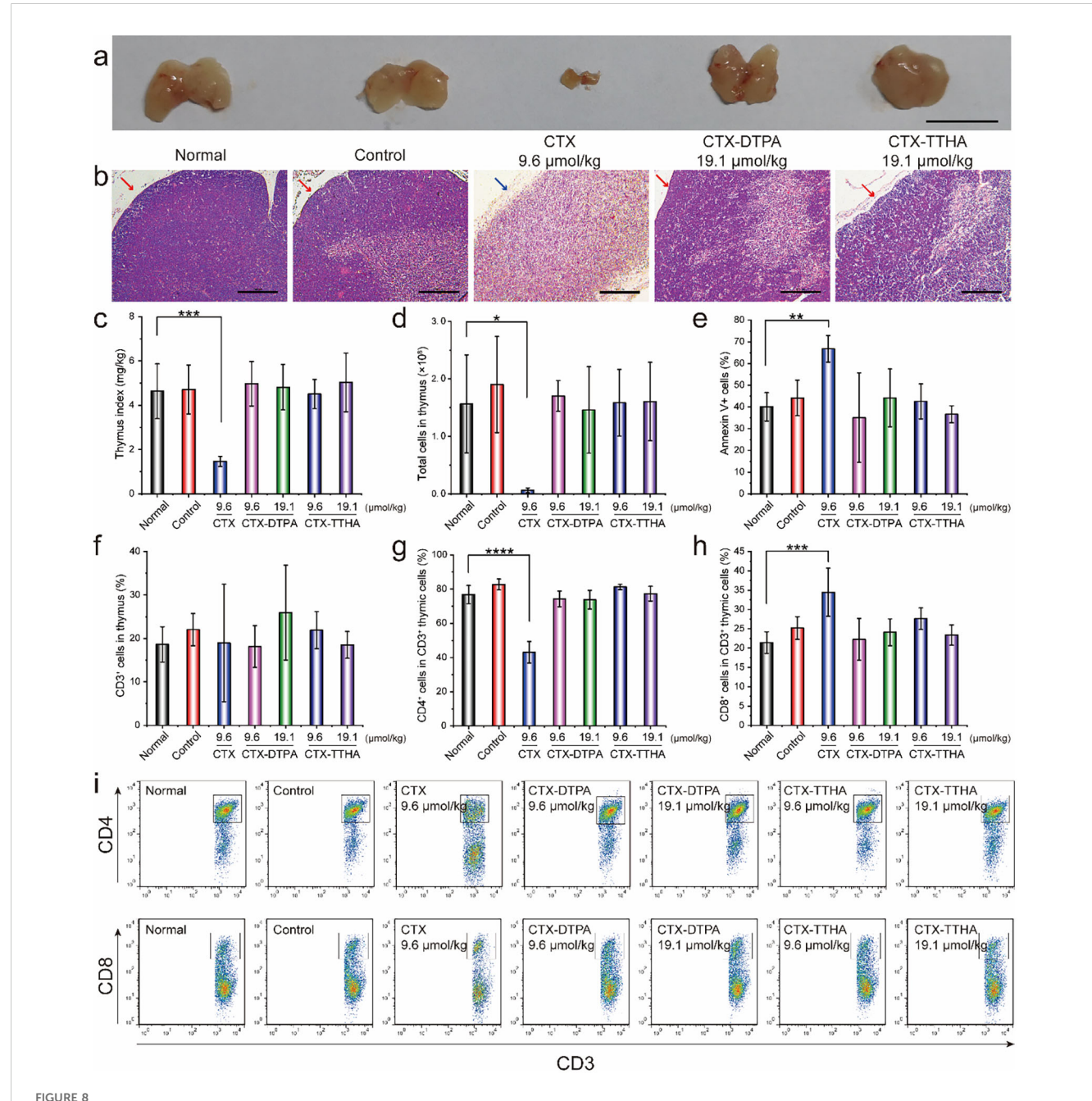


The effect of CTXs on H22 tumor-bearing mice. (a) Bodyweight changes. Liver (b) and spleen (c) indexes of mice in different groups (mean  $\pm$  SD, n=6). #p<0.05, ###p<0.001 vs. control group. (d) H&E staining of main organs. Blank arrows indicated the balloon-like hepatocytes with swollen volume and vacuolar cytoplasm. The boundary of the red and white pulp of spleens (yellow circles). Yellow arrows indicated the increased macrophages. Scale bar, 100  $\mu$ m. WBC (e) and lymphocyte (f) cell counts on day 7 and day 15. Data was presented as mean  $\pm$  SD, n=6, \*p < 0.05 vs. normal group, \*\*p<0.01 vs. normal group.

Hematological analysis revealed that CTX caused severe myelosuppression, reducing white blood cell counts to  $1.55 \pm 0.17 \times 10^9$ /L (vs 4.46  $\pm$  1.19×10 $^9$ /L in controls, p<0.01) on day 7 post-treatment. Importantly, CTX-DTPA and CTX-TTHA maintained near-physiological hematological parameters throughout the treatment period, with WBC counts ranging from 3.50- $5.60 \times 10^9$ /L across all dose groups (Figures 7e, f). This preservation of bone marrow function represents a critical therapeutic advantage over conventional CTX therapy.

# 2.9 Thymic preservation and immunocompatibility

The thymoprotective properties of CTX-DTPA and CTX-TTHA emerged as particularly noteworthy findings. While CTX administration resulted in profound thymic atrophy (31% of normal weight, p<0.05) and cortical depletion, both derivatives maintained normal thymic architecture with intact cortical-medullary differentiation (Figures 8a-c). Flow cytometric analysis



The effect of CTXs on the thymus in mice bearing H22 tumors. (a) Images of the thymus after 2 weeks of treatment. Scale bar, 1 cm. (b) H $\theta$ E staining analysis of the thymus. The red arrow indicated the cortex of the thymus, and the blue arrow indicated the missing cortex. Scale bar, 100  $\mu$ m. (c) Thymus index (mg/g). (d) Cell numbers of the thymus in different groups. (e) The apoptotic cells of the thymus were analyzed by flow cytometry. (f) The percentage of CD3<sup>+</sup> thymic cells. The proportion of CD4<sup>+</sup> (g) and CD8<sup>+</sup> cells (h) in CD3<sup>+</sup> thymic cells. (i) The distribution of CD4<sup>+</sup> and CD8<sup>+</sup> cells in CD3<sup>+</sup> thymic cells. Data was presented as mean  $\pm$  SD. n=6. \*p<0.05, \*\*p<0.01, \*\*\*p<0.001, \*\*\*\*p<0.0001 vs. normal group.

confirmed the preservation of thymocyte populations (Figures 8d, f), with apoptosis rates in derivative-treated groups (35.1-44.2%) remaining comparable to controls and significantly lower than CTX-treated animals (66.8%, p<0.05) (Figure 8e). Furthermore, the modified compounds prevented the CTX-induced disruption of CD4<sup>+</sup>/CD8<sup>+</sup> T cell ratios, maintaining the physiological balance critical for immune competence (Figures 8g-i).

These collective findings demonstrate that polycarboxylate modification successfully dissociates the antitumor efficacy of cabazitaxel from its dose-limiting toxicities, particularly the hematological and immunological adverse effects that have constrained clinical utility. The preservation of thymic structure and function suggests these derivatives may offer unique advantages for combination with emerging immunotherapies, potentially addressing a significant unmet need in contemporary cancer treatment paradigms.

To assess whether the preserved thymic architecture and cellularity translated to systemic immune homeostasis, we analyzed T-cell populations in the peripheral blood. Flow cytometric analysis revealed that the ratios of CD4<sup>+</sup> and CD8<sup>+</sup> T cells in all treatment

groups, including those administered unmodified CTX, were comparable to those in normal, healthy mice (Supplementary Figure S5). This finding indicates that, at the time of measurement, the peripheral T-cell pool remained stable across all groups despite the severe thymic damage induced by CTX.

# 2.10 Pharmacokinetic and biodistribution profiles of CTX and CTX-DTPA

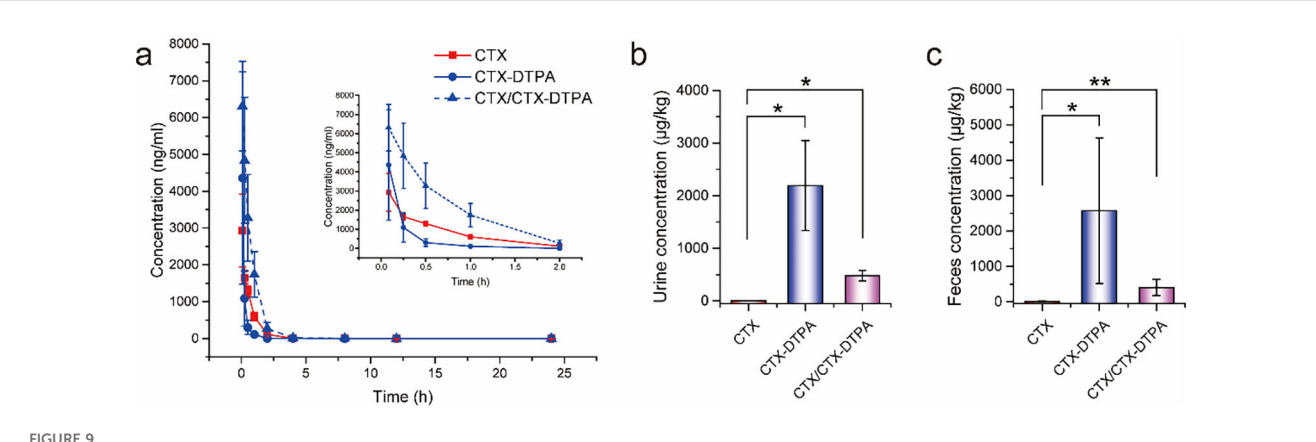
The pharmacokinetic analysis revealed distinct profiles between CTX and its water-soluble derivative CTX-DTPA following intravenous administration (6  $\mu$ mol/kg) in SD rats. CTX-DTPA demonstrated significantly prolonged systemic exposure compared to the parent compound, exhibiting a 5.1-fold longer elimination half-life (6.44  $\pm$  0.00 h  $\nu$ s. 1.27  $\pm$  0.09 h; p < 0.0001) and higher plasma exposure of the active metabolite CTX (CTX/CTX-DTPA) (AUC: 5157.71  $\pm$  1650.87  $\nu$ s. 1679.81  $\pm$  193.83  $\mu$ g/L•h; p < 0.0001) (Table 2, Figure 9a). The derivative showed rapid conversion to active CTX, achieving a 2.2-

TABLE 2 Non-compartmental model parameters.

Parameters	Units	CTX group	CTX-DTPA group	
		СТХ	CTX-DTPA	CTX/CTX-DTPA
C <sub>max</sub>	μg/L	2931.67 ± 989.53	4356.67 ± 2881.79	* 6311.67 ± 1217.79
t <sub>1/2</sub>	Н	1.27 ± 0.09	**** 6.44 ± 0.00	**** 2.77 ± 0.00
AUC <sub>0-t</sub>	μg/L*h	1679.81 ± 193.83	1334.61 ± 776.86	**** 5157.71 ± 1650.87
MRT <sub>0-t</sub>	Н	0.67 ± 0.09	1.04 ± 0.57	0.72 ± 0.02
CL	L/h/kg	3.01 ± 0.34	* 7.53 ± 4.66	1.51 ± 0.41
V <sub>d</sub>	L/kg	5.53 ± 0.81	*** 69.93 ± 43.28	* 6.04 ± 1.63

Cmaxo maximum concentration; t<sub>1/2</sub>, half time; AUC, area under concentration-time curve; MRT, mean residence time, MMRT; CL, Clearance; V<sub>d</sub>, apparent volume of distribution.

Data was presented as mean  $\pm$  SD, n=6.



Pharmacokinetic and excretion profiles of CTX-DTPA versus CTX in SD rats. (a) Plasma concentration-time curves showing prolonged circulation of CTX-DTPA and its metabolite CTX/CTX-DTPA (6  $\mu$ mol/kg IV dose). (b) Cumulative urinary excretion. (c) Cumulative fecal excretion. Data demonstrate enhanced elimination of CTX-DTPA (80% total excretion in 24 h) compared to CTX (<1%). Data was presented as mean  $\pm$  SD (n=6). \*p < 0.05 vs. CTX group, \*\*p < 0.01 vs. CTX group.

CTX: Drug concentration of cabazitaxel in the CTX treatment group.

CTX-DTPA: Concentration of the parent drug CTX-DTPA in the CTX-DTPA treatment group.

CTX/CTX-DTPA: CTX metabolite derived from CTX-DTPA biotransformation.

<sup>\*</sup>p<0.05, \*\*\*p<0.001, \*\*\*\*p<0.0001 vs. CTX.

fold greater Cmax (6311.67  $\pm$  1217.79 vs. 2931.67  $\pm$  989.53  $\mu$ g/L), suggesting sustained drug release characteristics.

Both CTX-DTPA and its metabolite displayed markedly reduced tissue accumulation, with organ concentrations 10- to 100-fold lower than CTX across all examined tissues (Table 3). Particularly notable differences were observed in the thymus (0.62  $\pm$  0.05 vs. 87.84  $\pm$  23.46 µg/kg at 15 min; p < 0.01) and spleen (0.39  $\pm$  0.04 vs. 249.73  $\pm$  38.31 µg/kg at 15 min; p < 0.001), demonstrating substantially diminished off-target tissue distribution.

The markedly reduced tissue accumulation of CTX-DTPA and its metabolite, particularly in immune organs like the thymus and spleen (Table 3), can be primarily attributed to its enhanced systemic clearance and high hydrophilicity, which limits passive diffusion into cells.

# 2.11 Excretion and safety profile

The excretion profiles differed dramatically between the two compounds. While CTX showed minimal elimination (<1% of dose in 24 h), CTX-DTPA exhibited rapid clearance with approximately 80% of the administered dose excreted within 24 hours, primarily through renal (39.8  $\pm$  12.7%) and fecal (43.5  $\pm$  32.8%) routes. The derivative's enhanced water solubility facilitated this efficient elimination, with urinary excretion dominated by intact CTX-DTPA (2191.14  $\pm$  853.66  $\mu g/kg)$  (Figure 9b) and fecal excretion containing both parent drug and metabolite (Figure 9c).

These results demonstrate that DTPA modification transforms the pharmacokinetic behavior of CTX, creating a compound with prolonged circulation, sustained release of the active drug, reduced

TABLE 3 Tissue distribution concentration (µg/kg).

Tissue	<b>T</b>	CTX group	CTX-DTPA group	CTX-DTPA group	
	Time	СТХ	CTX-DTPA	CTX/CTX-DTPA	
Thymus	15 min	87.84 ± 23.46	** 0.62 ± 0.05	** 1.49 ± 0.02	
	2 h	129.15 ± 50.01	* 0.10 ± 0.07	* 4.37 ± 5.02	
	4 h	109.86 ± 41.75	* 0.05 ± 0.01	* 0.79 ± 0.28	
	12 h	67.21 ± 4.15	**** 0.06 ± 0.04	**** 0.80 ± 0.42	
Heart	15 min	43.23 ± 12.9	* 0.27 ± 0.04	* 2.38 ± 0.46	
	2 h	24.56 ± 2.33	*** 0.07 ± 0.03	*** 2.27 ± 0.70	
	4 h	15.97 ± 1.91	*** 0.04 ± 0.00	*** 1.26 ± 0.20	
	12 h	12.59 ± 2.69	** 0.06 ± 0.03	** 0.41 ± 0.29	
	15 min	149.33 ± 7.27	*** 37.74 ± 16.89	*** 17.88 ± 1.12	
T.	2 h	78.73 ± 10.63	** 7.21 ± 1.30	** 10.31 ± 7.28	
Liver	4 h	48.74 ± 11.46	* 6.74 ± 5.04	** 4.62 ± 3.48	
	12 h	29.33 ± 11.48	* 0.65 ± 0.42	* 1.91 ± 1.12	
Spleen	15 min	249.73 ± 38.31	*** 0.39 ± 0.04	** 5.49 ± 0.53	
	2 h	159.81 ± 2.24	**** 0.09 ± 0.03	**** 8.23 ± 4.20	
	4 h	112.94 ± 21.04	** 0.05 ± 0.02	** 2.61 ± 0.42	
	12 h	54.03 ± 8.47	** 0.05 ± 0.03	** 1.43 ± 0.96	
Lung	15 min	132.60 ± 15.04	*** 2.36 ± 1.29	*** 12.95 ± 5.49	
	2 h	116.51 ± 4.61	**** 0.48 ± 0.50	**** 9.66 ± 5.84	
	4 h	106.75 ± 0.42	**** 0.13 ± 0.01	**** 2.44 ± 0.01	
	12 h	79.02 ± 30.87	* 1.10 ± 0.45	* 1.78 ± 0.82	
Kidney	15 min	549.67 ± 12.02	**** 41.08 ± 9.73	**** 53.38 ± 7.21	
	2 h	313.23 ± 47.52	** 4.96 ± 1.67	** 63.87 ± 43.92	
	4 h	307.73 ± 41.53	*** 1.55 ± 0.31	*** 8.74 ± 0.10	
	12 h	218.19 ± 15.93	**** 1.36 ± 0.84	**** 3.14 ± 1.66	

CTX: Drug concentration of cabazitaxel in the CTX treatment group.

Data was presented as mean  $\pm$  SD, n=6.

CTX-DTPA: Concentration of the parent drug CTX-DTPA in the CTX-DTPA treatment group.

 $<sup>\</sup>label{eq:ctx-dtp} \mbox{CTX/CTX-DTPA: CTX metabolite derived from CTX-DTPA biotransformation.}$ 

<sup>\*</sup>p<0.05, \*\*p<0.01, \*\*\*p<0.001, \*\*\*\*p<0.0001 vs. CTX.

tissue retention, and enhanced elimination clearance, which may translate to an improved therapeutic index and reduced systemic toxicity compared with those of the parent compound.

# 3 Discussion

The strategic redesign of cabazitaxel through polycarboxylic acid conjugation, resulting in CTX-DTPA and CTX-TTHA, represents a transformative approach that successfully decouples the potent antitumor efficacy of CTX from its dose-limiting systemic toxicities (25–31). Our findings comprehensively demonstrate that this chemical modification strategy not only conquers the fundamental challenge of aqueous solubility but also fundamentally reshapes the pharmacokinetic and safety profile of the drug, offering a promising path toward a safer and more immunocompatible chemotherapy (32, 33).

A pivotal and intriguing finding of our study is the resolved paradox between reduced target affinity and retained cytotoxicity. Molecular docking revealed that the polycarboxylate conjugation modestly reduced the binding affinity of the derivatives to β-tubulin. This apparent discrepancy, however, is convincingly explained by a multi-faceted compensatory mechanism. The dramatically improved hydrophilicity undoubtedly enhances drug availability and cellular uptake efficiency. More importantly, the tubulin polymerization assays indicated that the derivatives induce a distinct, more sustained microtubule stabilization pattern, resembling paclitaxel rather than the transient hyperpolymerization characteristic of native CTX (34). This suggests that the chemical modification has reprogrammed the drug's pharmacodynamic profile, leading to altered yet highly effective target engagement. Coupled with the efficient bioconversion to active metabolites observed in pharmacokinetic studies, these factors collectively ensure uncompromised antitumor potency.

The cornerstone of the clinical potential for CTX-DTPA and CTX-TTHA lies in their exceptionally enhanced safety profile (35, 36). The 64-fold improvement in hemocompatibility directly addresses the acute infusion-related toxicity of the clinical formulation. Furthermore, the mitigation of severe myelosuppression highlights a critical advantage over the parent compound. Perhaps the most significant advance is the pronounced thymoprotective effect. We observed that while unmodified CTX caused profound thymic atrophy and disrupted intrathymic T-cell development, our derivatives preserved the architectural and cellular integrity of this primary immune organ. This finding is of paramount importance, as the thymus serves as the factory for T-cell neogenesis (37). Its preservation is a fundamental prerequisite for long-term immune competence and resilience, a feature particularly crucial in the era of combination therapies with immunotherapies (37). The fact that our derivatives maintain a normal peripheral T-cell profile further supports that the central protection of the thymus successfully translates to systemic immune homeostasis.

The remarkably reduced tissue accumulation, especially in the thymus and spleen, provides the mechanistic underpinning for the observed immunocompatibility and reduced organ toxicity. As elucidated by our pharmacokinetic data, this phenomenon is primarily driven by the synergistic effect of enhanced systemic clearance and reduced passive cellular uptake due to the high hydrophilicity of the conjugates. This altered biodistribution is a direct result of our chemical design strategy, which strategically avoids the extensive tissue retention of the highly lipophilic parent drug.

From a pharmaceutical development perspective, our direct chemical conjugation strategy offers distinct advantages over conventional nanocarrier-based delivery systems. It bypasses challenges such as drug leakage, low loading capacity, carrier-related immunogenicity, and manufacturing inconsistencies. The synthesis is reproducible, yields a well-defined molecular entity, and results in a formulation that is stable in aqueous solution. The successful dissociation of efficacy from toxicity achieved here underscores the power of rational molecular design over complex physical encapsulation for optimizing cytotoxic agents.

In conclusion, this study establishes polycarboxylic acid conjugation as a robust and transformative strategy for revitalizing cabazitaxel. The derivatives CTX-DTPA and CTX-TTHA embody a unique combination of water solubility, potent and sustained antitumor activity, and a markedly improved safety profile encompassing hematological and immunological protection. The mechanistic insights into their altered tubulin interaction and favorable pharmacokinetics challenge conventional structure-activity relationship paradigms. Future work will focus on further structural refinements and evaluating the potential of these immunocompatible derivatives in combination with modern immunotherapies. This approach paves the way for a new generation of chemotherapeutic agents designed for both uncompromising efficacy and system-wide safety.

# Data availability statement

The original contributions presented in the study are included in the article/Supplementary Material. Further inquiries can be directed to the corresponding author.

# **Ethics statement**

The animal study was approved by Animal Ethics Committee of the Chinese Academy of Medical Sciences and Peking Union Medical College. The study was conducted in accordance with the local legislation and institutional requirements.

# **Author contributions**

LM: Conceptualization, Data curation, Funding acquisition, Methodology, Writing – original draft. YZ: Data curation, Methodology, Writing – original draft. NZ: Data curation, Writing – original draft. XW: Data curation, Writing – original draft. TL: Conceptualization, Funding acquisition, Supervision, Writing – review & editing.

# **Funding**

The author(s) declare financial support was received for the research and/or publication of this article. This study was supported by the Tianjin Key Technology R&D Program (20YFZCSY00570), the National Major Science and Technology special project for "significant new drugs development" (2018ZX09711001-005-018), the CAMS Innovation Fund for Medical Sciences (2021-I2M-1-015), the CAMS Fundamental Research Funds for the Central universities (3332018120).

# Conflict of interest

The authors declare that the research was conducted in the absence of any commercial or financial relationships that could be construed as a potential conflict of interest.

# Generative AI statement

The author(s) declare that no Generative AI was used in the creation of this manuscript.

Any alternative text (alt text) provided alongside figures in this article has been generated by Frontiers with the support of artificial intelligence and reasonable efforts have been made to ensure accuracy, including review by the authors wherever possible. If you identify any issues, please contact us.

# Publisher's note

All claims expressed in this article are solely those of the authors and do not necessarily represent those of their affiliated organizations, or those of the publisher, the editors and the reviewers. Any product that may be evaluated in this article, or claim that may be made by its manufacturer, is not guaranteed or endorsed by the publisher.

# Supplementary material

The Supplementary Material for this article can be found online at: https://www.frontiersin.org/articles/10.3389/fimmu.2025.1680710/full#supplementary-material

# References

- 1. Zhang Y, Zhang W, Wang Y, Zhu J, Zhou M, Peng C, et al. Emerging nanotaxanes for cancer therapy. *Biomaterials*. (2021) 272:120790. doi: 10.1016/j.biomaterials.2021.120790
- 2. Chen R, Cheng Q, Owusu-Ansah KG, Chen J, Song G, Xie H, et al. Cabazitaxel, a novel chemotherapeutic alternative for drug-resistant hepatocellular carcinoma. *Am J Cancer Res.* (2018) 8:1297–306.
- 3. Cao X, Li B, Chen J, Dang J, Chen S, Gunes EG, et al. Effect of cabazitaxel on macrophages improves CD47-targeted immunotherapy for triple-negative breast cancer. *J Immunother Cancer*. (2021) 9:e00202. doi: 10.1136/jitc-2020-002022
- 4. Chen Y, Dai L, Shi K, Pan M, Yuan L, Qian Z. Cabazitaxel-loaded thermosensitive hydrogel system for suppressed orthotopic colorectal cancer and liver metastasis. Advanced Sci (Weinheim Baden-Wurttemberg Germany). (2024) 11:e2404800. doi: 10.1002/advs.202404800
- 5. Kommineni N, Mahira S, Domb AJ, Khan W. Cabazitaxel-loaded nanocarriers for cancer therapy with reduced side effects. *Pharmaceutics*. (2019) 11:141. doi: 10.3390/pharmaceutics11030141
- Galsky MD, Dritselis A, Kirkpatrick P, Oh WK. Cabazitaxel. Nat Rev Drug Discov. (2010) 9:677–8. doi: 10.1038/nrd3254
- 7. Pan L, Schneider F, Ottenbruch M, Wiechert R, List T, Schoch P, et al. A general strategy for the synthesis of taxane diterpenes. *Nature*. (2024) 632:543–9. doi: 10.1038/s41586-024-07675-8
- 8. Lv H, Jia W, Yang L, Dong P, Liu J, Wang S, et al. Influence of unsaturated fatty acids on the antitumor activity of polymeric conjugates grafted with cabazitaxel against prostate cancer. *Biomedicine pharmacotherapy = Biomedecine pharmacotherapie*. (2023) 169:115902. doi: 10.1016/j.biopha.2023.115902
- 9. Cheng Y, Ou Z, Li Q, Yang J, Hu M, Zhou Y, et al. Cabazitaxel liposomes with aptamer modification enhance tumor–targeting efficacy in nude mice. *Mol Med Rep.* (2019) 19:490–8. doi: 10.3892/mmr.2018.9689
- 10. Zhao Z, Li Y, Liu H, Jain A, Patel PV, Cheng K. Co-delivery of IKBKE siRNA and cabazitaxel by hybrid nanocomplex inhibits invasiveness and growth of triple-negative breast cancer. *Sci Adv.* (2020) 6:eabb0616. doi: 10.1126/sciadv.abb0616
- 11. Shao Y, Zhang C, Yao Q, Wang Y, Tian B, Tang X, et al. Improving cabazitaxel chemical stability in parenteral lipid emulsions using cholesterol. *Eur J Pharm Sci.* (2014) 52:1–11. doi: 10.1016/j.ejps.2013.09.024
- 12. Jin J, Wan J, Hu X, Fang T, Ye Z, Wang H. Supramolecular nanoparticles self-assembled from reduction-responsive cabazitaxel prodrugs for effective cancer therapy. *Chem Commun (Cambridge England)*. (2021) 57:2261–4. doi: 10.1039/D0CC06854C
- 13. Bteich J, Ernsting MJ, Mohammed M, Kiyota T, McKee TD, Trikha M, et al. Nanoparticle formulation derived from carboxymethyl cellulose, polyethylene glycol,

- and cabazitaxel for chemotherapy delivery to the brain. *Bioconjugate Chem.* (2018) 29:2009–20. doi: 10.1021/acs.bioconichem.8b00220
- 14. Sun Y, Lee RJ, Meng F, Wang G, Zheng X, Dong S, et al. Microfluidic self-assembly of high cabazitaxel loading albumin nanoparticles. *Nanoscale.* (2020) 12:16928–33. doi: 10.1039/C9NR10941B
- 15. Wan Z, Xie F, Wang L, Zhang G, Zhang H. Preparation and evaluation of cabazitaxel-loaded bovine serum albumin nanoparticles for prostate cancer. *Int J nanomedicine*. (2020) 15:5333–44. doi: 10.2147/IJN.S258856
- 16. Zhang Y, Song W, Geng J, Chitgupi U, Unsal H, Federizon J, et al. Therapeutic surfactant-stripped frozen micelles. *Nat Commun.* (2016) 7:11649. doi: 10.1038/ncomms11649
- 17. Parhizkar E, Samani SM, Sakhteman A, Daneshamouz S, Parhizkar G, Ahmadi F. Synthesis, cytotoxicity assay, pharmacokinetics, biodistribution and modeling study of cabazitaxel-dextran nanoconjugates: targeted vs non targeted delivery. *Colloids surfaces. B Biointerfaces.* (2022) 209:112187. doi: 10.1016/j.colsurfb.2021.112187
- 18. Hyldbakk A, Fleten KG, Snipstad S, Åslund AKO, Davies CL, Flatmark K, et al. Intraperitoneal administration of cabazitaxel-loaded nanoparticles in peritoneal metastasis models. *Nanomedicine*. (2023) 48:102656. doi: 10.1016/j.nano.2023.102656
- 19. Ren L, Xu P, Yao J, Wang Z, Shi K, Han W, et al. Targeting the mitochondria with pseudo-stealthy nanotaxanes to impair mitochondrial biogenesis for effective cancer treatment. ACS nano. (2022) 16:10242–59. doi: 10.1021/acsnano.1c08008
- 20. Zhu N, Meng S, Mao L, Rong Y, Wang X, Liu Y, et al. Amino polycarboxylic acids-modified abiraterone derivatives as potential injectable anti-prostate cancer agents. *Bioorg Chem.* (2024) 153:107824. doi: 10.1016/j.bioorg.2024.107824
- 21. Chen Y, Deng Y, Zhu C, Xiang C. Anti prostate cancer therapy: Aptamer-functionalized, curcumin and cabazitaxel co-delivered, tumor targeted lipid-polymer hybrid nanoparticles. *Biomedicine pharmacotherapy = Biomedecine pharmacotherapie*. (2020) 127:110181. doi: 10.1016/j.biopha.2020.110181
- 22. Mu M, Liang X, Chuan D, Zhao S, Yu W, Fan R, et al. Chitosan coated pH-responsive metal-polyphenol delivery platform for melanoma chemotherapy. *Carbohydr polymers.* (2021) 264:118000. doi: 10.1016/j.carbpol.2021.118000
- 23. Wu S, Lu L, Zhou J, Ran D, Wang S, Xu Q, et al. All-stage targeted therapy for glioblastoma based on lipid membrane coated cabazitaxel nanocrystals. *J Controlled release.* (2022) 345:685–95. doi: 10.1016/j.jconrel.2022.03.047
- 24. Zhu L, Zhang C, Lü X, Song C, Wang C, Zhang M, et al. Binding modes of cabazitaxel with the different human  $\beta$ -tubulin isotypes: DFT and MD studies. *J Mol modeling*. (2020) 26:162. doi: 10.1007/s00894-020-04400-w

25. Wan J, Huang L, Cheng J, Qi H, Jin J, Wang H. Balancing the stability and drug activation in adaptive nanoparticles potentiates chemotherapy in multidrug-resistant cancer. *Theranostics.* (2021) 11:4137–54. doi: 10.7150/thno.54066

- 26. Oudard S, Ratta R, Voog E, Barthelemy P, Thiery-Vuillemin A, Bennamoun M, et al. Biweekly vs triweekly cabazitaxel in older patients with metastatic castration-resistant prostate cancer: the CABASTY phase 3 randomized clinical trial. *JAMA Oncol.* (2023) 9:1629–38. doi: 10.1001/jamaoncol.2023.4255
- 27. Sun Y, Zhao Y, Teng S, Hao F, Zhang H, Meng F, et al. Folic acid receptor-targeted human serum albumin nanoparticle formulation of cabazitaxel for tumor therapy. *Int J nanomedicine*. (2019) 14:135–48. doi: 10.2147/IJN.S181296
- 28. Agema BC, Buck SAJ, Viskil M, Isebia KT, de Neijs MJ, Sassen SDT, et al. Early identification of patients at risk of cabazitaxel-induced severe neutropenia. *Eur Urol Oncol.* (2024) 7:786–93. doi: 10.1016/j.euo.2023.10.015
- 29. Xu H, Zuo S, Wang D, Zhang Y, Li W, Li L, et al. Cabazitaxel prodrug nanoassemblies with branched chain modifications: Narrowing the gap between efficacy and safety. *J Controlled release.* (2023) 360:784–95. doi: 10.1016/j.jconrel.2023.07.012
- 30. Li J, Zeng H, You Y, Wang R, Tan T, Wang W, et al. Active targeting of orthotopic glioma using biomimetic liposomes co-loaded elemene and cabazitaxel modified by transferritin. *J nanobiotechnology*. (2021) 19:289. doi: 10.1186/s12951-021-01048-3
- 31. Carolina Cruz de Sousa A, da Silva Santos E, da Silva Moreira T, Gabriela Araújo Mendes M, Rodrigues Arruda B, de Jesus Guimarães C, et al. Anti-EGFR immunoliposomes for cabazitaxel delivery: From formulation development to *in vivo*

- evaluation in prostate cancer xenograft model. Int J Pharm. (2024) 661:124439. doi: 10.1016/j.ijpharm.2024.124439
- 32. Chen C, Fan R, Wang Y, Wang L, Huang C, Zhou L, et al. Hyaluronic acid-conjugated nanoparticles for the targeted delivery of cabazitaxel to CD44-overexpressing glioblastoma cells. *J Biomed nanotechnology.* (2021) 17:595–605. doi: 10.1166/jbn.2021.3050
- 33. Wang J, Li J, Wu Y, Xu X, Qian X, Lei Y, et al. ROS-responsive nanocomplex of aPD-L1 and cabazitaxel improves intratumor delivery and potentiates radiation-mediated antitumor immunity. *Nano Lett.* (2022) 22:8312–20. doi: 10.1021/acs.nanolett.2c03227
- 34. Serpico AF, Pisauro C, Grieco D. cGAS-dependent proinflammatory and immune homeostatic effects of the microtubule-targeting agent paclitaxel. *Front Immunol.* (2023) 14:1127623. doi: 10.3389/fimmu.2023.1127623
- 35. Sun B, Lovell JF, Zhang Y. Current development of cabazitaxel drug delivery systems, Wiley interdisciplinary reviews. *Nanomedicine nanobiotechnology*. (2023) 15: e1854. doi: 10.1002/wnan.1854
- 36. Sun B, Paraskevopoulos G, Min J, Rossdeutcher R, Ghosh S, Quinn B, et al. Topical drug delivery of concentrated cabazitaxel in an  $\alpha$ -tocopherol and DMSO solution. Advanced Sci (Weinheim Baden-Wurttemberg Germany). (2023) 10:e2302658. doi: 10.1002/advs.202302658
- 37. Taves MD, Ashwell JD. Glucocorticoids in T cell development, differentiation and function, Nature reviews. *Immunology*. (2021) 21:233–43. doi: 10.1038/s41577-020-00464-0